話題・解説 (II)

2021 年度核データ部会賞

奨励賞

Neutron Beam Filter System for Fast Neutron Cross-Section Measurement at the ANNRI Beamline of MLF/J-PARC

日本原子力研究開発機構
核データ研究グループ
Rovira Leveroni, Gerard
gerard.rovira@jaea.go.jp

1. Introduction

Precise nuclear data for minor actinides (MAs) and fission products (FPs) are of the utmost important for the design of advanced nuclear facilities and, hence, incessant experimental efforts are necessary in order to continuously improve the nuclear data accuracy. The Accurate Neutron-Nucleus Reaction Measurement Instrument (ANNRI) beamline in the Materials and Life Science Experimental Facility (MLF) building of the Japan Proton Accelerator Research Complex (J-PARC) was designed for such endeavor. Since its inception in 2010, several measurement campaigns have been carried out using the experimental equipment currently installed at ANNRI: (1) a 4π high-purity Ge detector array, (2) a NaI(Tl) spectrometer and (3) two Li-glass detectors. Thus far, the reported accurate experimental results for neutron-induced reactions include data for the neutron total and neutron capture cross section for MAs such as ^{241}Am [1], ^{243}Am [2] and ^{237}Np [3, 4]; FP including ^{99}Tc [5] and ^{107}Pd [6]; and structural material, namely ^{93}Nb [7] and ^{181}Ta [8]. Current research trends, which are focused on the nuclear transmutation of high-level nuclear waste (HLW), require further experimental data for MAs in the keV-region [9, 10]. Nonetheless, the present status of the ANNRI beamline does not allow for cross section results to be attained without substantial ambiguities for keV-neutron induced reactions. The reason for this is the operation pattern of the J-PARC accelerator. In the current condition, the J-PARC accelerator is operated in the double-bunch mode in which two proton bunches are shot into the spallation target with a time difference of 0.6 μs at 25 Hz. For keV neutron induced reactions, the 0.6 μs time difference between spallation reactions is not negligible since it is within one order of magnitude of the neutron time-of-flight (TOF), e.g., 100 keV neutrons have a TOF of 6.4 μs and, moreover, it is not

possible to ascertain whether the detected events were induced by neutrons originated in the primary or the delayed spallation reaction. Thus, it is imperative for the ambiguities introduced by the double-bunch mode to be resolved in order for accurate experimental results in the keV region to be attainable again. In this article, the main viewpoints of the neutron filtering system implemented at ANNRI are presented. A complete assessment of the neutron filtering system can be found here [11, 12].

2. Neutron Filtering Technique

The neutron filtering technique has been applied to the ANNRI beamline in order to tailor quasi-monoenergetic neutron beams to bypass the double-bunch structure of the incident neutron beam. This technique is based on employing thick slabs of materials that possess the characteristic of a sharp minima in the neutron total cross section. By designing the filtering system with the adequate thickness, neutron with energies other than that of the sharp minima are stopped in the filter material. Hence, only neutrons with the energies of the sharp minima are able to stream through the filter material creating mono-energetic neutron beams. This technique has been successfully applied to continuous neutron sources such as nuclear reactors [13, 14, 15] and in one TOF experiment [16]. In the present work, the neutron filtering technique was applied to the ANNRI beamline to resolve the double-bunch predicament in keV-neutron experiments. Three different filter configurations with 20 cm of ^{nat}Fe, 20 cm of ^{nat}Si and 15 cm ^{nat}Cr were analyzed separately with expected filtered energies of 24 keV (Fe), 54 and 144 keV (Si); and 46 and 136 keV (Cr). The neutron total cross sections for ^{nat}Fe, ^{nat}Si and ^{nat}Cr from JENDL-4.0 [17] are displayed in Fig. 1 together with the neutron energies of the sharp minima.

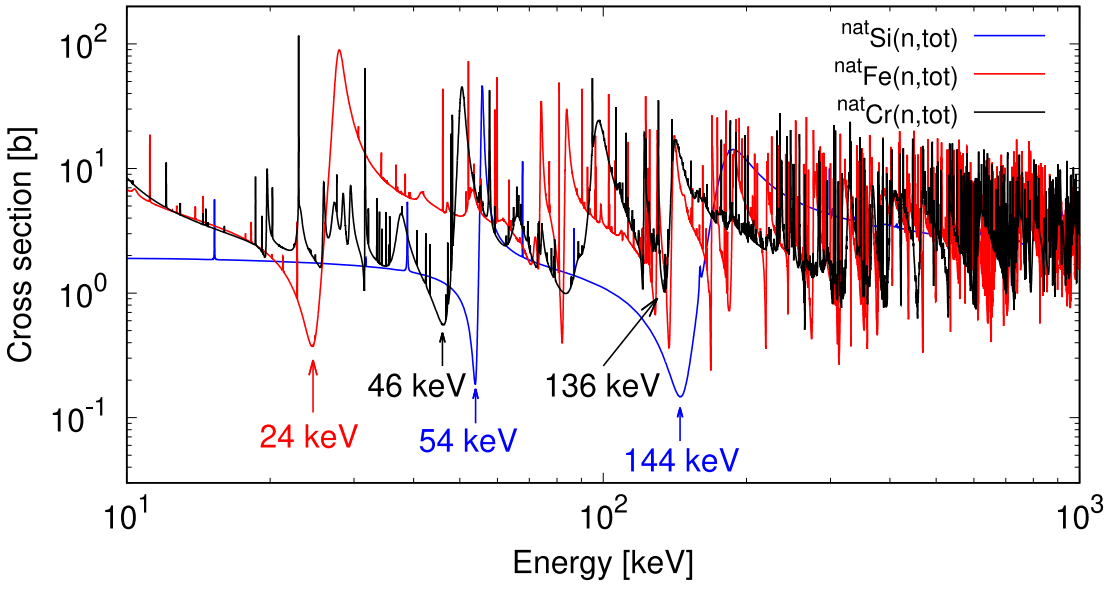

Fig. 1 Neutron total cross sections of ^{nat}Fe, ^{nat}Si and ^{nat}Cr from JENDL-4.0.

3. Experimental Setup

The performance of the neutron filter was evaluated by means of neutron capture and transmission experiments using the NaI(Tl) spectrometer and the Li-glass detectors installed in the ANNRI beamline, respectively. The filter materials were introduced into the rotary collimator of the ANNRI beamline, right before the experimental areas. The position of the neutron filter relative to the detectors can be seen in the schematics of the ANNRI beamline in Fig. 2.

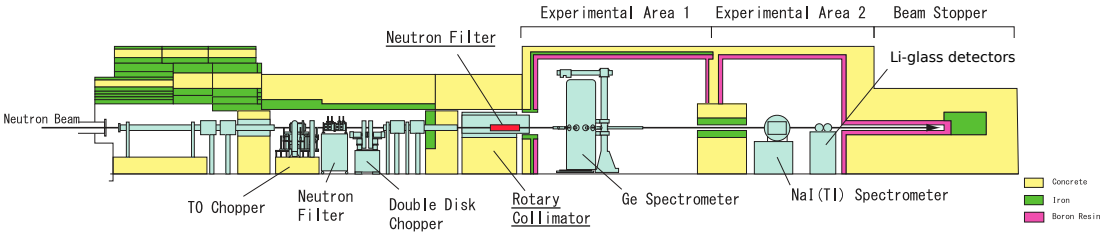

Fig. 2 Schematic of the ANNRI beamline.

3.1 Neutron Capture Experiments

The time distribution of the filtered incident neutron flux was experimentally determined by measuring the 478-keV γ-rays emitted from the ^{10}B(n,$\alpha\gamma$)^{7}Li reaction in a measurement of a 90%-enriched ^{10}B sample with a diameter of 10 mm and a thickness of 0.5 mm. This technique is commonly used in the ANNRI beamline since this reaction emits only one γ-ray and, thus, detected events from the ^{10}B(n,$\alpha\gamma$)^{7}Li reaction are easy to isolate. The detected events were first corrected using the simulations with the PHITS code [18] taking into account the ^{10}B(n,$\alpha\gamma$)^{7}Li energy dependence and other sample related effects such as self-shielding and multiple scattering and, then, normalized by means of the saturated resonance method using a measurement of a Au sample thick enough for the first resonance to be completely saturated. Further information about the neutron capture experimental setup can be found here [3].

3.2 Neutron Transmission Experiments

The neutron capture experiments were complemented with neutron transmission experiments in order to increase the reliability of the present study since this is the first time that the neutron filtering technique is applied to the ANNRI beamline. Therefore, the filtered neutron time distribution was experimentally determined with the Li-glass detectors as well. Two Li-glass detectors with different concentrations of Li were employed. A GS20 detector having a ^{6}Li $> 95\%$ concentration was utilized to measure the filtered neutron TOF spectrum by means of the ^{6}Li(n, α)^{3}H reaction. Moreover, a GS30 detector with a concentration of ^{7}Li $> 99\%$ was also used to estimate the background contribution due to other particles aside from neutrons. A complete description of the Li-glass detectors setup of the ANNRI beamline is provided here [1].

4. Experimental Results

The experimental neutron time distribution results were determined using the NaI(Tl) spectrometer and the Li-glass detectors installed in the ANNRI beamline. As shown in Fig. 3, there is very good agreement with the results from both detector setups for the three filter configurations. The only difference arises due to the different detector position relative to the spallation target. The NaI(Tl) spectrometer is situated at a neutron flight path of 27.9 m whereas the Li-glass detectors are situated at a neutron flight path of 28.6 m and, hence, results from the Li-glass detectors present some delay relative to the NaI(Tl) spectrometer results. Nonetheless, all the expected filtered peaks for the three filter configurations of 24 keV (Fe), 54 and 144 keV (Si); and 46 and 136 keV (Cr) are clearly visible with both detector setups.

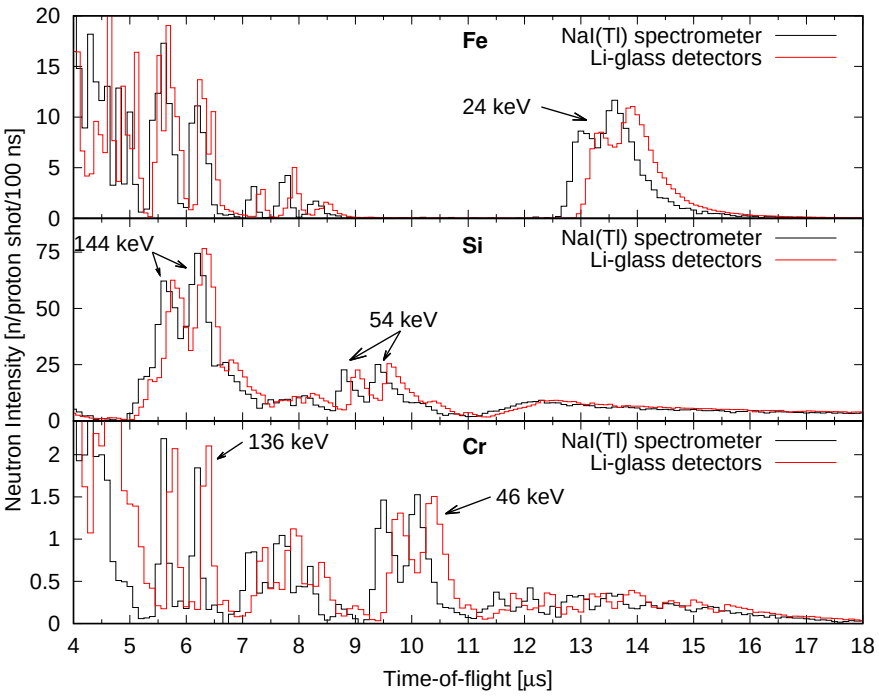

Fig. 3 Filtered neutron time distribution measured with the NaI(Tl) spectrometer (black) and the Li-glass detectors (red) for the filter configurations of 20 cm of ^{nat}Fe (top), 20 cm of ^{nat}Si (middle) and 15 cm of ^{nat}Cr (bottom).

5. Monte-Carlo Simulations

Even though the expected peaks for the three filter assemblies are clearly distinguishable from the background levels, the neutron energy distribution within the filtered peaks cannot be directly ascertained from the neutron TOF because the direct relationship between neutron TOF and energy is hampered by the double-bunch mode. In order to determine the neutron energy distributions, Monte-Carlo simulations with the PHITS code were performed to reproduce the experimental neutron time distribution results. The neutron transmission ratios were simulated with PHITS and the

results were unfolded by applying the ANNRI resolution function from the work of Kino *et al.* [19] using the model function proposed by Ikeda and Carpenter [20].

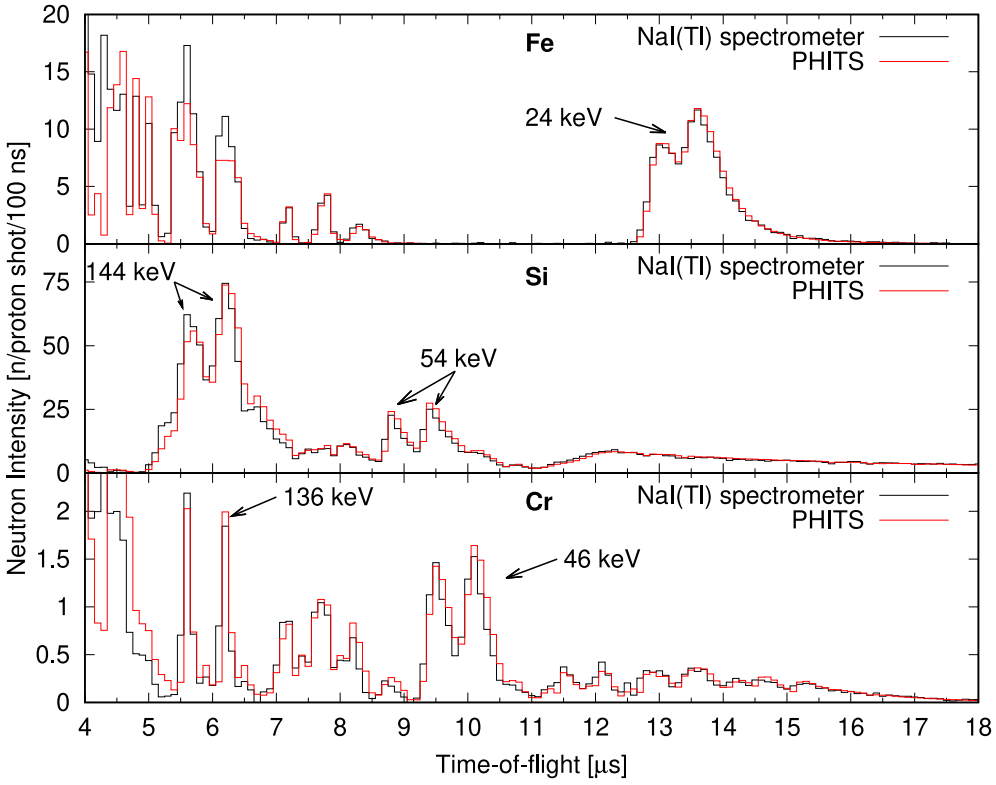

Fig. 4 Simulated filtered neutron time distribution with PHITS (red) compared with the experimental results obtained with the NaI(Tl) spectrometer (black) for the filter configurations of 20 cm of ^{nat}Fe (top), 20 cm of ^{nat}Si (middle) and 15 cm of ^{nat}Cr (bottom).

Two-dimensional results for the neutron time and energy distributions were obtained simultaneously from the Monte-Carlo simulations. With the aim of assessing the reliability of the simulations, the simulated neutron time distribution results were compared to those obtained from the experimental neutron capture measurements. As can be seen in Fig. 4, the simulated results are able to accurately reproduce the experimental filtered neutron time distribution results obtained with the NaI(Tl) spectrometer. At the same time, since neutron time and energy distributions were simultaneously calculated and, taking into consideration that the simulated neutron time distributions precisely reproduce the experimental results, the simulated neutron energy distributions are deemed highly reliable and, thus, were employed to determine the neutron energy distribution within the filtered peaks.

The energy distribution results for the Fe assembly are displayed in Fig. 5. A TOF gate was created from 12.6 to 15.0 μs to wrap the simulated events streamed through the 24 keV window and the results showed a neutron energy distribution within the filtered peak with a centroid energy of 23.5 keV. By using the neutron filtering system it is clear that a much sharper neutron energy distribution is obtained, eliminating the contribution from higher and lower energy neutrons.

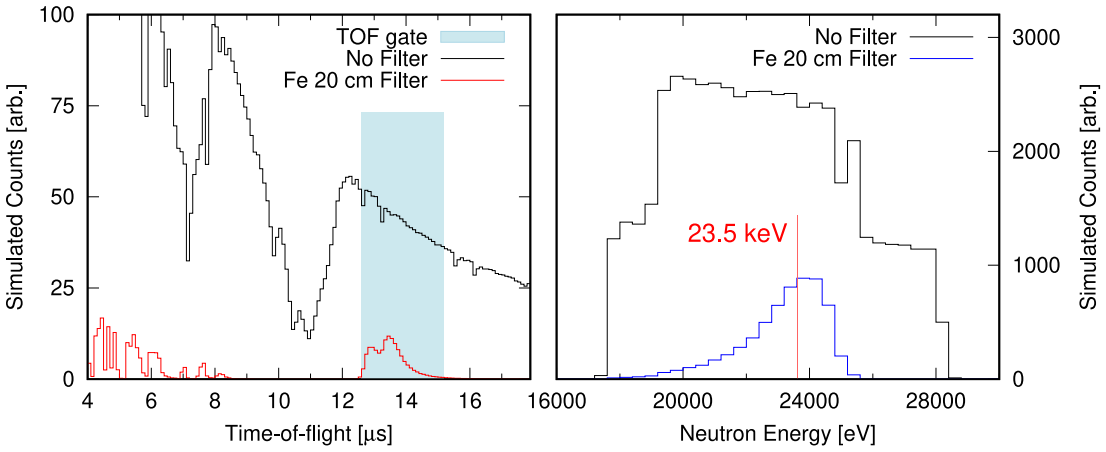

Fig. 5 (left) Simulated filtered TOF spectrum by the Fe filter assembly (red) compared to the TOF from the simulation without filter (black). A TOF gate was created between 12.6 and 15.0 μs (light blue). (right) Simulated energy distribution of the gated neutrons from 12.6 to 15.0 μs for the Fe filter array (blue) and the simulation with no filter (black).

Similar filtering performances for the remaining filtered peaks from the Si and Cr filter assemblies were obtained. The Si filter simulation yielded much sharper neutron energy distributions with centroid energies of 127.7 keV and 51.5 keV as shown in Figs. 6 and 7. The results of 127.7 keV are much lower than the expected value of 144 keV. This is due to the influence of the ^{nat}Al present in the beamline. ^{nat}Al possesses high values for the neutron total cross section around 140 to 150 keV and, hence, neutrons with that energy are not able to reach the sample position of the NaI(Tl) spectrometer as they interact with the ^{nat}Al present in the beamline.

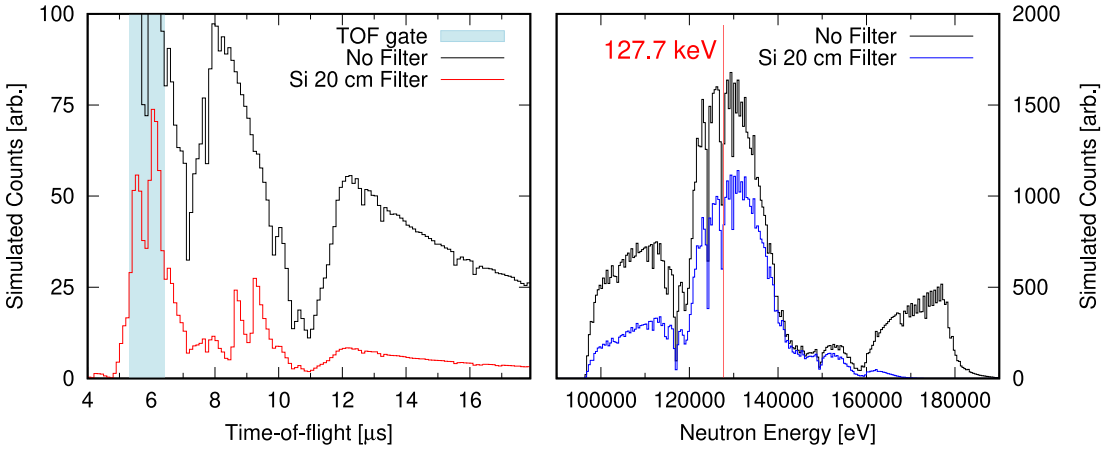

Fig. 6 (left) Simulated filtered TOF spectrum by the Si filter assembly (red) compared to the TOF from the simulation without filter (black). A TOF gate was created between 5.4 and 6.4 μs (light blue). (right) Simulated energy distribution of the gated neutrons from 5.4 and 6.4 μs for the Si filter array (blue) and the simulation with no filter (black).

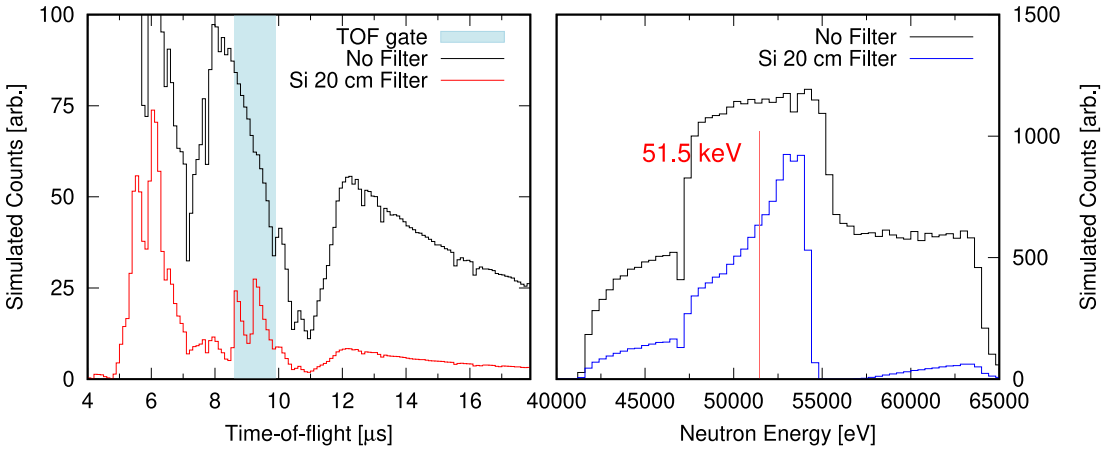

Fig. 7 (left) Simulated filtered TOF spectrum by the Si filter assembly (red) compared to the TOF from the simulation without filter (black). A TOF gate was created between 8.6 and 9.8 μs (light blue). (right) Simulated energy distribution of the gated neutrons from 8.6 and 9.8 μs for the Si filter array (blue) and the simulation with no filter (black).

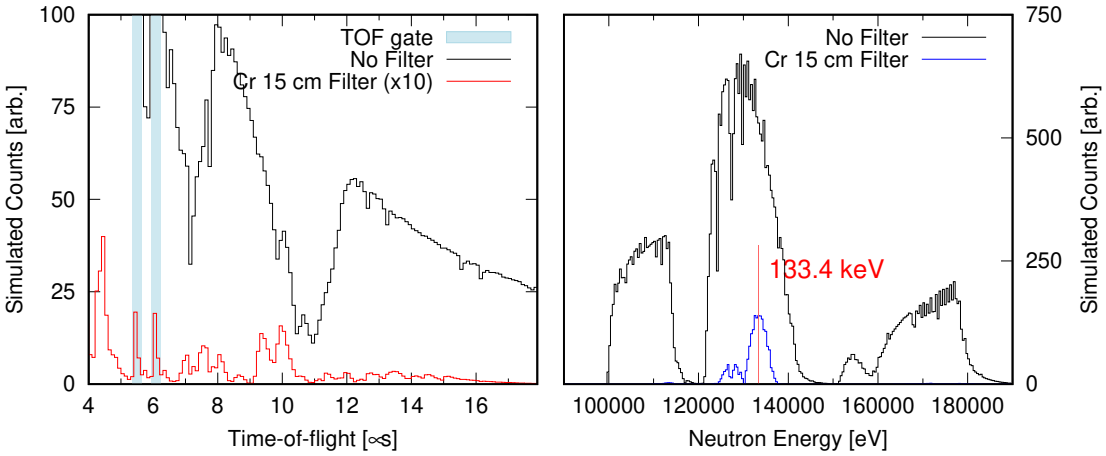

Fig. 8 (left) Simulated filtered TOF spectrum by the Cr filter assembly (red) compared to the TOF from the simulation without filter (black). A TOF gate was created from 5.4 to 5.7 and 6.0 to 6.3 μs (light blue). (right) Simulated energy distribution of the gated neutrons within 5.4 to 5.7 and 6.0 to 6.3 μs for the Si filter array (blue) and the simulation with no filter (black).

Finally, the neutron energy distribution obtained from the simulations of the Cr filter array are presented in Figs. 8 and 9. Centroid energies of 133.4 and 45.0 keV were determined from the analysis of the simulation results. The neutron energy distribution results are summarized in Table 1 including the obtained standard deviations for the neutron energy distribution within the each filtered peak.

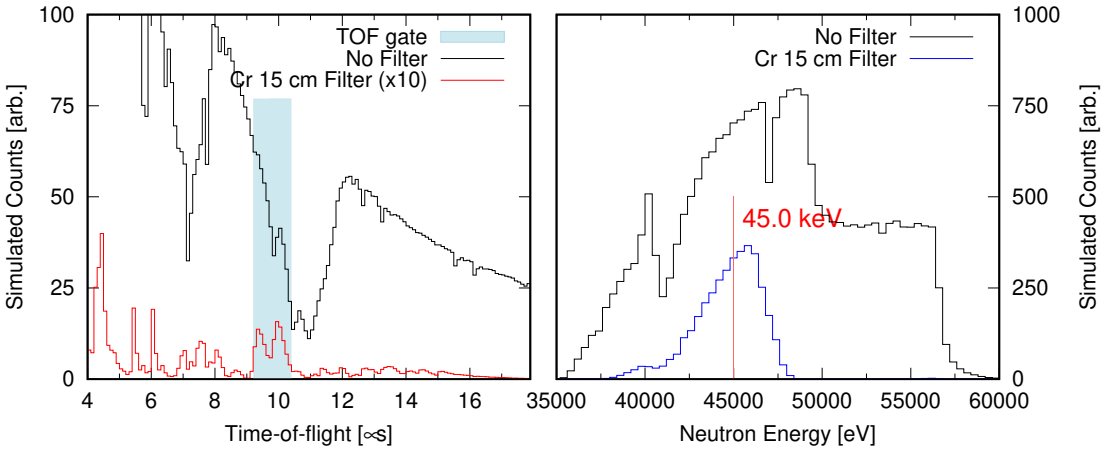

Fig. 9 (left) Simulated filtered TOF spectrum by the Cr filter assembly (red) compared to the TOF from the simulation without filter (black). A TOF gate was created between 9.2 to 10.5 μs (light blue). (right) Simulated energy distribution of the gated neutrons from 9.2 to 10.5 μs for the Si filter array (blue) and the simulation with no filter (black).

Table 1 Summary of the performance for the different filters analyzed.

Filter Element	Centroid Energy [keV]	Std. dev [keV]
Fe	23.5	1.4
Si	51.5	3.9
	127.7	12.5
Cr	45.0	1.9
	133.4	8.1

6. Standard Cross Section Measurement

The neutron filtering system performance in neutron capture cross section experiments was evaluated by means of standard cross section measurements. Evaluated nuclear data from the ^{197}Au(n,γ)^{198}Au reaction is deemed highly reliable due to the large amount of experimental data available. Thus, experimental techniques can be assessed by referring the experimental value for the ^{197}Au(n,γ)^{198}Au reaction to the standard evaluated nuclear data. In the present work, the neutron capture cross section of ^{197}Au was determined at each of the five filtered peaks tailored by the neutron filtering system with centroid energies of 23.5 keV (Fe), 51.5 and 127.7 keV (Si); and 45.0 and 133.4 keV (Cr). The neutron capture cross section was calculated by creating TOF gates to wrap the events of each of the filtered peaks as follows:

$$\langle \sigma_{Au}(E_g) \rangle = \frac{Y_{Au}(E_g) C(E_g)}{\phi_n(E_g)} \frac{1}{n_{Au}} \quad (1)$$

where $< \sigma_{Au}(E_g) >$ is the averaged neutron capture cross-section for each of the five TOF gates (E_g); $Y_{Au}(E_g)$ and $C(E_g)$ are the Au neutron capture yield and the correction coefficient for self-shielding and multiple-scattering for each TOF gate (E_g), respectively. $\phi_n(E_g)$ stands for the

normalized incident neutron flux at the TOF gate (E_g) and n_{Au} sample area density in at/barn.

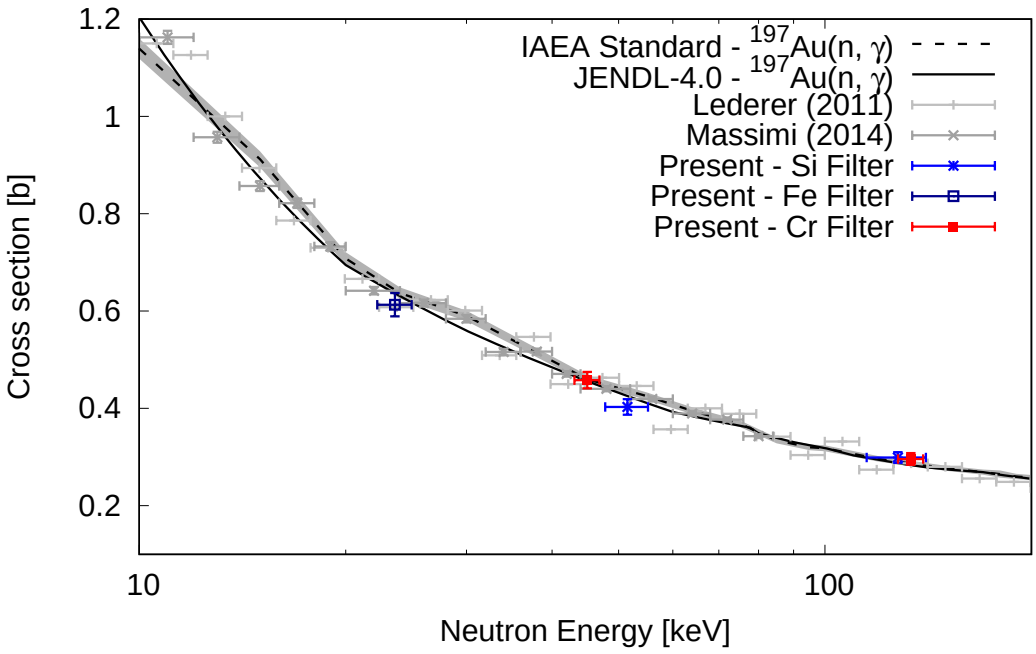

Fig. 10 Neutron capture cross-section results for ^{197}Au using the filter configurations of 15 cm of Cr (45.0 and 133.4 keV), 20 cm of Fe (23.5 keV) and 20 cm of Si (51.5 and 127.7 keV) as filter material compared with the evaluated data from JENDL-4.0 and the IAEA standard data library with uncertainty; and with the experimental data reported by Ledererd and Massimi.

The results for the neutron capture cross-section of ^{197}Au are shown in Fig. 10 together with the evaluated data from JENDL-4.0 [17] and the IAEA standard cross section[21]: and the reported data from Lederer [22] and Massimi[23]. The x-axis bars mean the standard deviation displayed in Table 1. The present cross-section results are consistent with the experimental data from Lederer and Massimi and agree within one-sigma uncertainty with both evaluated nuclear data values from JENDL-4.0 and IAEA standard cross section library. The present results provide evidence that keV-neutron capture cross section measurements are attainable at the ANNRI beamline by using the neutron filtering system to bypass the double-bunch structure of the incident neutron beam.

7. Conclusions

A neutron filtering system has been installed at the ANNRI beamline in order to accurately measure neutron-induced cross sections in the keV region avoiding the ambiguities introduced by the double-bunch structure of the incident neutron beam. The neutron filtering system consists of a series of thick cylinders made of materials that possess the characteristic of sharp minima in the neutron total cross section. In the present study, the filtering performance of three filter configurations consisting of 20 cm of ^{nat}Fe, 20 cm of ^{nat}Si and 15 cm of ^{nat}Cr was experimentally examined

by means of neutron capture and transmission experiments. These results were complemented by Monte-Carlo simulations with the PHITS code. These filter configurations are able to mold the incident neutron flux into sharp neutron peaks with centroid energies of 23.5 keV (Fe), 51.5 and 127.7 keV (Si); and 45.0 and 133.4 keV (Cr). Moreover, the effectiveness in keV-neutron capture cross section measurements was validated by the good agreement of the present experimental results of the ^{197}Au(n,γ)^{198}Au reaction using the neutron filtering system with the evaluated nuclear data values from JENDL-4.0 and the IAEA standard cross section library, together with the reported data of Lederer and Massimi. Thus, in this work, the neutron filtering technique was proved to be a suitable solution to avoid the influence of the double-bunch structure of the incident neutron flux in order to accurately measure keV-neutron-induced reactions.

8. Acknowledgments

The neutron experiments at the MLF of the J-PARC were performed under the user program (Proposal No. 2018A0213, 2018B0195, 2020P0100 and 2020A0273). This work is supported by the Innovative Nuclear Research and Development Program from the Ministry of Education, Culture, Sports, Science and Technology of Japan. Grant Number: JPMXD0217942969.

References

[1] Terada K et al., J. Nucl. Sci. Technol. 2018; 55:1198-1211.

[2] Kimura A et al., J. Nucl. Sci. Technol. 2019; 56:479-492.

[3] Rovira G et al., J. Nucl. Sci. Technol. 2020; 57:24-39.

[4] Rovira G et al., J. Nucl. Sci. Technol. 2022; 59:110-122.

[5] Katabuchi T et al., EPJ Web of Conf. 2017; 146:11050.

[6] Terada K et al., Prog. in Nucl. Energ. 2015; 82:118-121.

[7] Endo S et al., J. Nucl. Sci. Technol. 2021;1-16.

[8] Endo S et al., J. Nucl. Sci. Technol. 2022 [In production].

[9] Salvatores M et al., OECD, 2008; NEA No. 6410.

[10] Iwamoto H et al., Nuclear Data Sheets, 2014; 118:519-522.

[11] Rovira G et al., Nucl. Inst. and Meth. in Phys. Res. A, 2021. 1003-165318.

[12] Rovira G et al., J. Nucl. Sci. Technol. 2022 [In production].

[13] Tsang FY et al., Nucl. Inst. and Meth., 1976; 134:441-447.

[14] Košťál M et al., Appl. Rad. and Isot., 2017; 128:41-48.

[15] Greenwood RC et al., Nucl. Inst. and Meth., 1976; 138:125-143.

[16] McDermott BJ et al., Phys. Rev. C, 2017; 96-014607.

[17] Shibata K et al., J. Nucl. Sci. Technol, 2011. 48:1–30

[18] T. Sato et al., J. Nucl. Sci. Technol. 2018; 55:684-690.

[19] Kino K et al., Nucl. Inst. and Meth. in Phys. Res. A, 2014; 736:66-74.

[20] Ikeda S et al., Nucl. Inst. and Meth. in Phys. Res. A, 1985; 239:536-544.

[21] Carlson AD et al., Nucl Data Sheets, 2018; 149:143-188.

[22] Lederer C et al., Phys. Rev. C, 2011; 83:034608.

[23] Massimi C et al., Eur. Phys. J. A, 2014; 50:124.